Compressible Octave Spanning Supercontinuum Generation by Two-Pulse Collisions

Ayhan Demircan*
Institute for Quantum Optics, Leibniz Universität Hannover, Welfengarten 1, 30167 Hannover, Germany

Shalva Amiranashvili and Carsten Brée
Weierstrass Institute for Applied Analysis and Stochastics, Mohrenstraße 39, 10117 Berlin, Germany

Günter Steinmeyer
Max-Born-Institut, Max-Born-Straße 2A, 12489 Berlin, Germany and Optoelectronics Research Centre, Tampere University of Technology, 33101 Tampere, Finland
(Received 20 December 2012; published 4 June 2013)

We demonstrate a novel method for supercontinuum generation in an optical fiber based on two-color pumping with a delay and a group velocity matching. The scheme relies on the enhanced cross-phase-modulation at an intensity induced refractive index barrier between a dispersive wave and a soliton. The generation mechanism neither incorporates soliton fission nor a modulation instability and therefore exhibits extraordinary coherence properties, enabling the temporal compression of octave bandwidth into a short pulse. Moreover, the properties of the supercontinuum are adjustable over a wide range in the frequency domain by suitable choice of the dispersive wave.

DOI: 10.1103/PhysRevLett.110.233901 PACS numbers: 42.65.Re, 42.65.Ky, 42.65.Tg, 42.81.Dp

With the advent of microstructured fibers [1], white-light supercontinuum (SC) generation [2] became possible at nanojoule pulse energies from laser oscillators. Microstructure fibers enable generation of octave-spanning optical fields, which revolutionized frequency metrology [3] and are highly interesting for spectroscopy, optical communications, and medical imaging [4,5]. Soliton fission (SF) was identified as the key mechanism behind this remarkably efficient SC generation process [6]. Here, the decay of initial high-power pulses into a train of fundamental solitons is accompanied by the generation of dispersive waves (DW) and leads to rapid spectral broadening.

SF comes with a severe disadvantage, namely, its poor spectral coherence properties [7]. Despite its impressive spectral coverage, the optical field often proves incompressible in the temporal domain [8,9]. This loss of spectral coherence shapes out as highly irregular pulse trains that do not reproduce from shot to shot. In this situation, temporal compression requires adaptive dispersion control with MHz update rates. Moreover, spectral broadening in the anomalous dispersion regime makes SC generation highly susceptible to laser noise as the latter is always amplified via the inherent modulation instability (MI) [2,10]. Therefore, although octave-spanning SC generation is routine nowadays, there still appears to be room for improvement on how to provide ultrawide spectra fulfilling the challenging demands on the source characteristics [11–13]. Low spectral coherence can certainly be avoided in the normal dispersion regime, where both SF and MI are suppressed. Here, complicated pulse shapes stemming from nondeterministic temporal pulse splitting do not appear, which suitably avoids spectrally varying modulations. However, now the spectral broadening is mainly induced by self-phase-modulation and the Raman effect, enabling comparatively modest spectral broadening. Therefore, it appears appealing to combine the enormous spectral coverage of soliton-based SC sources with the superior coherence properties in the normal-dispersion regime.

In the following, we devise a SC generation mechanism for microstructured waveguide devices that is totally independent of SF and MI. With efficiencies comparable to that of SF, our suggested mechanism effectively avoids the problem of poor spectral coherence, which promises the generation of compressible octave-spanning SC. Our technique relies on resonant two-color excitation based on the elementary cross-phase-modulation (XPM) interaction [14]. At first sight, this may appear similar to two-color high-harmonic generation [15], yet it borrows from the repulsion phenomenon between a soliton and a DW packet only possible in the fiber geometry. This repulsion results from an impenetrable intensity induced refractive index barrier for the DW, as has been demonstrated in fiber Bragg gratings [16,17], photonic crystal fibers [18], and for two-beam collisions [19,20] and is also at the heart of the concept of the fiber optical analogue of an event horizon [21–25]. All these demonstrations inherently rely on the fact that optical media enable synchronous propagation and effective interaction of a soliton in the anomalous dispersion regime together with a DW packet in the normal dispersion regime [26].

For modeling SC generation induced by two pulses with considerably different carrier frequencies, we avoid the slow-envelope description and deal with the full analytic signal $\mathcal{E}(z, t)$ of the real-valued field $E(z, t)$, where

$\mathcal{E}(z,t) = 2\sum_{\omega>0} E_\omega(z) e^{-i\omega t}$ is a sum of all positive-frequency spectral components. The analytic signal is governed by a Schrödinger-type unidirectional equation

$$\partial_z \mathcal{E} + \hat{\beta}\mathcal{E} + \frac{n_2}{c}\partial_t[(1-f_R)|\mathcal{E}|^2\mathcal{E} + f_R\mathcal{E}\hat{h}|\mathcal{E}|^2]_+ = 0. \quad (1)$$

Here, $\hat{\beta}$ and $\hat{h}$ denote convolution with the propagation constant $-i\beta(\omega)$ and the Raman term $(\nu_1^2+\nu_2^2)/[\nu_1^2-(\omega+i\nu_2)^2]$, respectively. We employ $\nu_1^{-1} = 12.2$ fs, $\nu_2^{-1} = 32$ fs, $f_R = 0.18$. Only positive-frequency parts of the nonlinear term $[]_+$ are accounted for, and the term $\mathcal{E}^*\hat{h}\mathcal{E}^2$ is neglected. Equation (1) is similar to the unidirectional model for the real-valued field [6], yet with the added benefit of a clear separation from third harmonic generation (THG), the latter being described by inclusion of the term $\mathcal{E}^3$ [27]. In a traditional formulation [2], one employs the parameter $\gamma = \omega_0 n_2 c^{-1} A_{\text{eff}}^{-1}(\omega_0)$, where ω_0 and $A_{\text{eff}}(\omega_0)$ refer to the carrier frequency and the corresponding mode area, respectively. For numerical estimates, we rescale $|\mathcal{E}|^2$ to instant power and use a typical value $\gamma = 0.1\ \text{W}^{-1}\,\text{m}^{-1}$.

The main prerequisite for our SC generation process is the buildup of an effective refractive index barrier [21,23]. This condition is best illustrated by example Fig. 1(c), where we first neglect the Raman effect for simplicity. Here, we simulated the interaction of a sech pulse with wavelength in the normal dispersion regime and a perfect

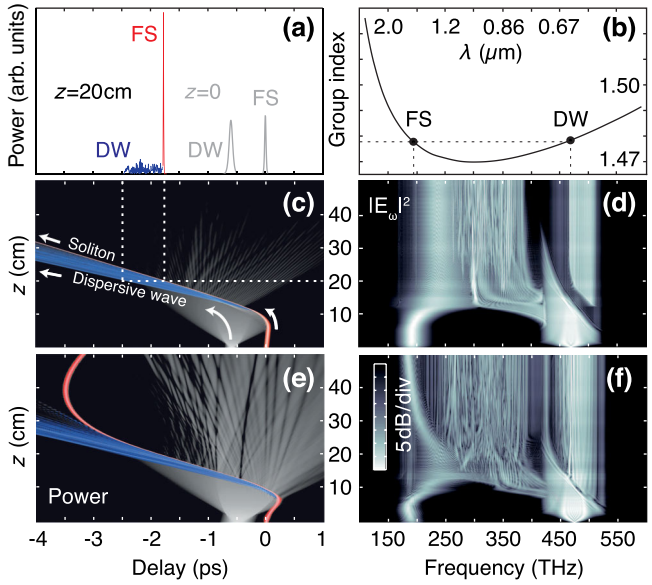

FIG. 1 (color online). Supercontinuum generation due to interaction of a fundamental soliton (FS) and a dispersive wave (DW) in a 5 μm silica strand in air. (a) Pulse profiles at $z = 0$ (gray) and $z = 20$ cm. (b) Fiber group index from Ref. [38] supports equal velocities of FS and DW. [(c)–(f)] Evolution in time and frequency domain (FS marked red and DW blue) without [(c), (d)] and with [(e), (f)] Raman effect. The dotted lines in (c) indicate a cross section shown in (a). Parameters in Table I.

fundamental soliton in the anomalous dispersion regime at a relative delay of 600 fs [gray line in Fig. 1(a)]. The initial wavelengths of the pulses ensure nearly identical group velocities [Fig. 1(b)]. The soliton maintains its shape during propagation [trajectory marked red in Figs. 1(c) and 1(e)]. However, the initially short normally dispersive pulse starts to temporally broaden within 5 cm of propagation length and subsequently interacts with the soliton via nonlinear refraction caused by an increase of the refractive index in the immediate surroundings of the soliton. This effect reduces group velocity, also affecting the dispersive radiation in this short temporal interval. For most parts of the dispersive radiation, the index modification presents a barrier that cannot be penetrated, as impressively demonstrated by the temporal power profile after 20 cm of propagation [red and blue lines in Fig. 1(a) and the vertical dashed line in Fig. 1(c)]. On a linear scale, there is virtually no radiation at delays greater than that of the soliton. Dispersive radiation colliding at the leading edge of the soliton strongly interacts with the soliton via XPM. As apparent in Figs. 1(d) and 1(f), this effect causes a blueshift of solitonic radiation and a converse effect for parts of the DW. These wavelength shifts also modify group velocities of the respective radiation parts, such that eventually some parts of the dispersive radiation [marked in blue in Figs. 1(c) and 1(e)] cannot cross the refractive index barrier induced by the soliton and are repelled from the soliton trajectory. Requiring only minor adjustment of input parameters, this repulsion works in the presence of the Raman effect equally well; see Figs. 1(e) and 1(f), respectively. In contrast to standard XPM [14], this mechanism can be exploited to manipulate properties of both pulses [26]. The accompanied acceleration of the soliton leads to a curved trajectory in the (t, z) plane even without Raman effect [Fig. 1(c)], as is typical for this kind of interaction [26,28,29].

Spectral broadening stems from different effects in the anomalous and normal dispersion regime. Due to XPM, the soliton experiences a frequency shift during copropagation. The interaction with the DW therefore transfers the soliton into a region with markedly decreased dispersion in Fig. 1(b). Due to the soliton area theorem, this effective change of dispersion leads to temporal compression of the soliton and to spectral broadening [28]. Similar adiabatic soliton compression is also exploited in dispersion-decreasing fibers (DDF), where a decrease of $\beta_2(z)$ is achieved by suitable tapering [14,30].

As soliton compression in DDF fibers also enables highly coherent spectral broadening in the anomalous dispersion regime [31], we simulated this method with parameters identical to those in Fig. 1; see Fig. 2. We gradually varied the dispersion from an initial value of -11.5 to -58 fs^2/mm [Fig. 2(d)]. The temporal compression of the soliton for linear and hyperbolic decreasing dispersion along z is shown in Fig. 2(a), leading to a

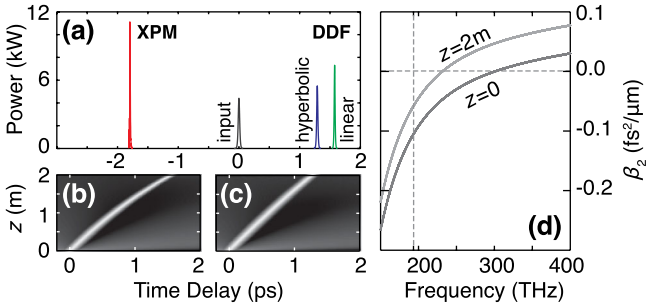

FIG. 2 (color online). (a) Temporal profiles of input and output pulses for linear and hyperbolic DDF, with XPM compressed fundamental soliton from Fig. 1(a) shown for comparison. [(b), (c)] Profile evolution along z for linear (b) and hyperbolic (c) DDF. (d) Group velocity dispersion vs frequency at both ends of the DDF. Vertical dotted line: soliton carrier frequency.

shortest pulse duration of 16.3 fs. Moreover, it requires much longer propagation to obtain this modest 1.7-fold compression whereas the XPM-based scheme enables compression to 5 fs within 20 cm propagation length; cf. pulse labeled XPM in Fig. 2(a). Another apparent disadvantage of soliton compression is the lack of direct control by the DW. Soliton compression requires a precast fabrication of a specific fiber dispersion profile. Finally, the XPM-based scheme additionally exhibits newly generated frequency components in the normal dispersion regime that stem from the reflection of the DW at the propagation front.

The spectrum in the normal dispersion regime consists of three different parts: (i) The spectrum of the initial DW, which is not reflected and passes the soliton. This part experiences only minor broadening by self-phase-modulation. (ii) Reflected DW portions. Upon propagation, nonlinear interaction accelerates the soliton, effectively feeding the interaction zone with a continuous supply of previously linearly propagating DW segments. As the frequency of the soliton increases, any of these interactions with DW segments creates new frequencies. This effect then eventually fills the entire spectral range between the DW and the zero dispersion frequency. (iii) Frequency components of the soliton that overlap the zero dispersion frequency and transfer energy to the normal dispersion regime. In the above example, the generated spectrum exhibits a 20-dB spectral width of 1050 nm, encompassing 1.5 octaves from 570 to 1620 nm.

It is known that the Raman effect is not detrimental for establishing a refractive index barrier [18,21,32] but may have a strong impact on the propagation dynamics. In the following, we investigate this impact on SC generation. Figures 1(e) and 1(f) show simulations including the Raman effect, corroborating that a very similar SC generation mechanism takes place here. However, DW parameters need to be adapted very carefully as the resonance condition depicted in Fig. 1(b) is continuously changed because the Raman effect affects the FS wavelength. The intensity and width of the DW are chosen to obtain a long interaction range by DW broadening. Sufficient SC buildup is ensured by choosing an appropriate time delay between the soliton and the DW. Yet, at the same time, the intensities of the DW portions at any collision point with the soliton have to be sufficiently high to overcome the counteracting deceleration by the self-frequency shift. This shift spectrally translates the soliton towards the red; cf. Fig. 1(e) at $z = 20$ cm and beyond. These modifications naturally suggest choosing group velocities of both pulses not too close to each other, which limits the range of suitable conditions for reflection. Nevertheless, provided suitable adjustment of pulse parameters, similar results for the SC with and without Raman scattering can be achieved [Figs. 1(e) and 1(f)], despite the significant impact of the Raman effect.

In order to demonstrate the possibilities for manipulating the SC characteristics, we performed numerous simulations with different pulse parameters (see Table I). The obtainable width of the SC is chiefly determined by the separation of the two initial frequencies, which enables optimization of the spectral width. Figure 3(a) impressively shows how adjustment of the amplitude of the DW may serve to fill the gap between the two input wavelengths, demonstrating a further advantage of our scheme. For a fixed frequency combination, the spectral width can be adjusted by the DW energy contents, and the SC can be tailored in different ways. As control parameters one can use the peak power, the pulse width of the DW, or the time delay between the DW and the soliton. More importantly, one can optimize the spectral bandwidth simply by suitable choice of the input frequency pair, as demonstrated by a bandwidth increase to 1.8 octaves in Fig. 3(b).

The importance of DWs has already been recognized in the traditional SC generation based on SF, where DWs lead

TABLE I. Pulse parameters. Both soliton and dispersive wave are assumed as $\sqrt{P}\cosh^{-1}(t/t_0)$, where P is the peak power.

	Soliton				Dispersive wave			
Figure	λ/nm	t_0/fs	P/kW	$\beta_2/(\mathrm{fs}^2/\mu\mathrm{m})$	λ/nm	t_0/fs	P/kW	$\beta_2/(\mathrm{fs}^2/\mu\mathrm{m})$
1(c), 1(d)	1550	15.5	4.4	−0.10	641	40	4.0	0.044
1(c), 1(d)	1550	15.5	4.4	−0.10	632	100	5.3	0.044
3(b), gray	1550	15.5	4.4	−0.10	632	100	5.3	0.046
Black	1666	15.5	5.0	−0.13	592	80	5.3	0.051

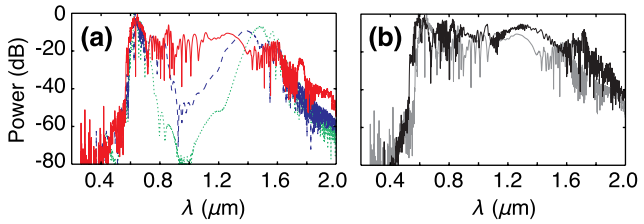

FIG. 3 (color online). SC adjustment by input pulse parameter variation. Spectra at $z = 12$ cm resulting (a) for collision of fundamental soliton with DWs with increasing peak power ($P = 4.0$, 4.4, 5.3 kW) and (b) for two different wavelength combinations. The width of the SC is determined by the initial frequency separation. See Table I for parameters.

to additional spectral broadening [23,29,33–35]. We stress that our scheme is markedly different from the previous SC generation scenario. We completely avoid the SF process as a generation mechanism, and Raman scattering is not a key factor either. We want to emphasize the difference between our scheme and other two-color pumping schemes where THG is responsible for the extension of the SC to shorter wavelengths [36]. Our model allows separate consideration of THG, and we actually observe only marginal affects by THG [Fig. 4(a), dotted green line]. In particular, we also see only minor differences when we change the relative phase between the two input pumps. Moreover, our scheme solely exploits four-wave mixing processes between two input pulses. This segregation prevents the decoherence problems seen in the traditional SC scheme. The spectral broadening avoids nondeterministic temporal pulse splitting, translating into spectral modulation and fluctuations. Also, the scheme does not exhibit a strong susceptibility to noise in the anomalous dispersion regime. Usually, noise is amplified in the input pulse through the MI, but as only one fundamental soliton with a short width is involved, the impact of MI is strongly reduced [10].

To demonstrate the superior coherence properties of our scheme, we calculate the modulus of the complex degree

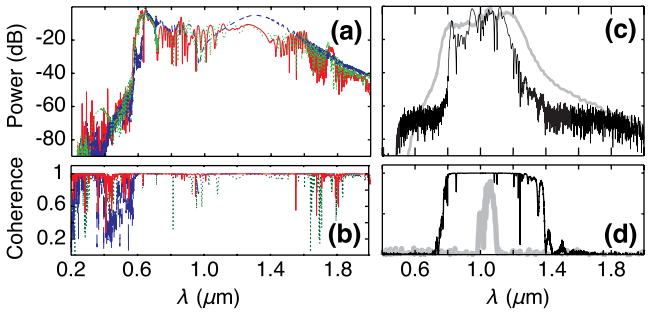

FIG. 4 (color online). (a) Spectra for the proposed SC generation scheme and (b) degree of coherence with (red solid line) and without (blue dashed line) Raman effect. The third-harmonic effect is shown by the dotted green line. (c) SC spectra by SF for soliton number $N = 15$ (black line) and $N = 40$ (gray line) and (d) corresponding degree of coherence.

of first-order coherence $|g_{12}(\lambda, t_1 - t_2)|$ [37] at each wavelength as a measure for the SC phase stability

$$g_{12}(\lambda, t_1 - t_2) = \frac{\langle \mathcal{E}_1^*(\lambda, t_1)\mathcal{E}_2(\lambda, t_2)\rangle}{\sqrt{\langle|\mathcal{E}_1(\lambda, t_1)|^2\rangle\langle|\mathcal{E}_2(\lambda, t_2)|^2\rangle}}, \quad (2)$$

where the angular brackets denote an ensemble average over 512 pairs of SC spectra, independently generated by using different quantum-limited shot noise seeds [2].

Figure 4(a) displays single-shot spectra at $z = 12$ cm for the examples presented in Fig. 1 with and without Raman gain. The degree of coherence seen in Fig. 4(b) indicates the expected sensitivity toward noise, with near-unity values promising perfect compressibility of SC spectra. In both cases, there is no appreciable coherence degradation within ≈ 1.5 octaves bandwidth. With the Raman effect, a stable SC is enabled when the self-frequency shift is sufficiently compensated by interaction with the DW, and we also observe degradation of the coherence with further propagation for that case. The nearly perfect coherence is slightly corrupted by contribution of the third harmonic [green dotted line in Fig. 4(b)].

To illustrate differences between resonant two-color SC generation and the standard SF method, we computed SF-based generation of a SC for comparison. Here, we inject a higher-order soliton at 290 THz, close to the zero dispersion wavelength into the fiber. Supercontinua for $N = 15$ (black line) and 40 (gray line) are shown in Fig. 4(c). A high degree of coherence is observed for low soliton orders at early stages of the SF process [Fig. 4(d), black line]. An increase of peak powers leads to a broader SC. This process eventually saturates [Fig. 4(c), gray line]. Despite comparatively low spectral coverage, MI clearly dominates this scenario, with SF-based continua eventually experiencing a complete coherence collapse [Fig. 4(d), gray line], ultimately thwarting their compression into a short pulse.

In conclusion, we presented a novel scheme for SC generation, which is based on the strong pulse reshaping only possible at soliton intensity induced refractive index barriers. Our method relies on soliton compression in combination with frequency conversion due to the reflection of DWs at the edge of a soliton. Besides the possibility to generate different spectral coverage ranges, favorable coherence properties can be achieved, and a negligible influence of input noise is demonstrated. The resulting SC covers more than an octave of compressible spectral content, which in principle, allows the synthesis of pulses in the single-cycle regime after suitable dispersion compensation. While such dispersion compensation will certainly turn out to be not trivial, a suitable device can be completely static, without the necessity of readjustments on a shot-to-shot basis. Moreover, the relatively smooth single-shot spectra generated by our method also appear appealing for applications. We therefore believe that our two-color scheme opens an avenue for new and previously impossible applications of supercontinua.

Sh. A. gratefully acknowledges support by the DFG Research Center MATHEON (Project No. D 14), and G. S. acknowledges support from the Academy of Finland (Project Grant No. 128844). A. D. acknowledges support by the DFG (Project No. MO 850/15-1).

*demircan@iqo.uni-hannover.de

[1] J. K. Ranka, R. S. Windeler, and A. J. Stentz, Opt. Lett. **25**, 25 (2000).
[2] J. M. Dudley, G. Genty, and S. Coen, Rev. Mod. Phys. **78**, 1135 (2006).
[3] S. T. Cundiff and Y. Je, Rev. Mod. Phys. **75**, 325 (2003).
[4] K. Saitoh and M. Koshiba, Opt. Express **12**, 2027 (2004).
[5] I. Hartl, X. D. Li, C. Chudoba, R. K. Ghanta, T. H. Ko, J. G. Fujimoto, J. K. Ranka, and R. S. Windeler, Opt. Lett. **26**, 608 (2001).
[6] A. V. Husakou and J. Herrmann, Phys. Rev. Lett. **87**, 203901 (2001).
[7] X. Gu, M. Kimmel, A. Shreenath, R. Trebino, J. Dudley, S. Coen, and R. Windeler, Opt. Express **11**, 2697 (2003).
[8] K. L. Corwin, N. R. Newbury, J. M. Dudley, S. Coen, S. A. Diddams, K. Weber, and R. S. Windeler, Phys. Rev. Lett. **90**, 113904 (2003).
[9] B. Schenkel, R. Paschotta, and U. Keller, J. Opt. Soc. Am. B **22**, 687 (2005).
[10] A. Demircan and U. Bandelow, Opt. Commun. **244**, 181 (2005); Appl. Phys. B **86**, 31 (2007).
[11] J. Bethge, A. Husakou, F. Mitschke, F. Noack, U. Griebner, G. Steinmeyer, and J. Herrmann, Opt. Express **18**, 6230 (2010).
[12] C. Ament, P. Polynkin, and J. V. Moloney, Phys. Rev. Lett. **107**, 243901 (2011).
[13] M. F. Saleh, W. Chang, J. C. Travers, P. St. J. Russell, and F. Biancalana, Phys. Rev. Lett. **109**, 113902 (2012).
[14] G. Agrawal, *Nonlinear Fiber Optics* (Academic, San Diego, 2001).
[15] I. J. Kim, C. M. Kim, H. T. Kim, G. H. Lee, Y. S. Lee, J. Y. Park, D. J. Cho, and C. H. Nam, Phys. Rev. Lett. **94**, 243901 (2005).
[16] C. M. De Sterke, Opt. Lett. **17**, 914 (1992).
[17] N. G. R. Broderick, D. Taverner, D. J. Richardson, M. Ibsen, and R. I. Laming, Phys. Rev. Lett. **79**, 4566 (1997).
[18] A. V. Gorbach and D. V. Skryabin, Opt. Express **15**, 14 560 (2007).
[19] N. Rosanov, JETP Lett. **88**, 501 (2008).
[20] V. E. Lobanov and A. P. Sukhorukov, Phys. Rev. A **82**, 033809 (2010).
[21] T. G. Philbin, C. Kuklewicz, S. Robertson, S. Hill, F. König, and U. Leonhardt, Science **319**, 1367 (2008).
[22] D. Faccio, Contemp. Phys. **53**, 97 (2012).
[23] D. V. Skryabin and A. V. Gorbach, Rev. Mod. Phys. **82**, 1287 (2010).
[24] A. Choudary and F. König, Opt. Express **20**, 5538 (2012).
[25] L. Tartara, IEEE J. Quantum Electron. **48**, 1439 (2012).
[26] A. Demircan, Sh. Amiranashvili, and G. Steinmeyer, Phys. Rev. Lett. **106**, 163901 (2011).
[27] Sh. Amiranashvili and A. Demircan, Phys. Rev. A **82**, 013812 (2010).
[28] A. Demircan, Sh. Amiranashvili, C. Brée, C. Mahnke, F. Mitschke, and G. Steinmeyer, Sci. Rep. **2**, 850 (2012).
[29] R. Driben, F. Mitschke, and N. Zhavoronkov, Opt. Express **18**, 25 993 (2010).
[30] K. R. Tamura and M. Nakazawa, IEEE Photonics Technol. Lett. **11**, 319 (1999).
[31] M. Nakazawa, K. Tamura, H. Kubota, and E. Yoshida, Opt. Fiber Technol. **4**, 215 (1998).
[32] S. Robertson and U. Leonhardt, Phys. Rev. A **81**, 063835 (2010).
[33] G. Genty, M. Lehtonen, and H. Ludvigsen, Opt. Express **12**, 4614 (2004).
[34] G. Genty, M. Lehtonen, and H. Ludvigsen, Opt. Lett. **30**, 756 (2005).
[35] T. Schreiber, T. Andersen, D. Schimpf, J. Limpert, and A. Tünnermann, Opt. Express **13**, 9556 (2005).
[36] G. Genty, P. Kinsler, B. Kibler, and J. M. Dudley, Opt. Express **15**, 5382 (2007).
[37] G. Genty, M. Surakka, J. Turunen, and A. T. Friberg, J. Opt. Soc. Am. B **28**, 2301 (2011).
[38] J. M. Stone and J. C. Knight, Opt. Express **16**, 2670 (2008).